HiSST: 2nd International Conference on
High-Speed Vehicle Science Technology
11–15 September 2022, Bruges, Belgium

Aerodynamic Characterization of STRATOFLY Hypersonic Vehicle by means of engineering methods and CFD simulations

Pietro Roncioni[1], Marco Marini[2], Roberta Fusaro[3], Nicole Viola[4]

Abstract

In the framework of European Commission Horizon2020 STRATOFLY Project, the aerodynamic characterization of external aeroshape of the hypersonic vehicle MR3 was conducted by means of engineering tools in order to rapidly sizing the control surfaces for stability and maneuverability all over the range of Mach number. One important aspect is the trimmability of the vehicle and so the correct dimensioning of longitudinal control surfaces. The results of this activity are presented in terms of global aerodynamic coefficients, control surfaces effects and stability derivatives. Sensitivity analysis with respect to the available engineering methods and comparisons with CFD simulations will be shown too, in order to provide reliable uncertainty ranges around the nominal data.

Keywords: *Hypersonic vehicle, Aerodynamics, Design, Flight Control*

1. Introduction

1.1. STRATOFLY Project

STRATOFLY is a highly-multidisciplinary project and is the most recent of a series of projects co-funded by the European Commission in the last fifteen years, combining technological and operative issues for hypersonic civil aircrafts and aiming to study the feasibility of high-speed passenger stratospheric flight. Technological, environmental, operational and economic factors, that allow the global sustainability of new air space's exploitation, are considered, drastically reducing transfer time (i.e. antipodal flights in less than two to four hours), emissions and noise, and guaranteeing the required safety levels. The main project objectives are to refine the design and the concept of operations of the LAPCAT-II MR2.4 vehicle, and to reach the ambitious goal of TRL=6 by 2035 for the concept, also considering that the crucial technologies of STRATOFLY vehicle may represent a step forward to reach the goal of future reusable space transportation systems.

1.2. Vehicle and mission description

The reference configuration for the STRATOFLY project is the LAPCAT-II MR2.4 vehicle, which is evolving towards to STRATOFLY MR3 vehicle (see Fig. 1) and has a length of 94 m, a wingspan of 41 m, a GTOW of 400 tons and carries 300 passengers. The configuration is a waverider aeroshape with a dorsal mounted combined propulsion system, i.e. a merging of six Air-Turbo-Rocket (ATR) engines, operating from take-off to Mach=4÷4.5, and one Dual-Mode-Ramjet (DMR) engine operating from Mach=4.5 to the cruise target Mach=8.

The reference antipodal flight trajectory is Brussels-Sydney with a hypersonic cruise at Mach 8 and 32÷33 km altitude, with a range of about 18700 km and a flight duration of about three hours (Fig 2).

[1] *CIRA, Italian Aerospace Research Centre, Via Maiorise, 81043 Capua - Italy, p.roncioni@cira.it*
[2] *CIRA, Italian Aerospace Research Centre, Via Maiorise, 81043 Capua - Italy, m.marini@cira.it*
[3] POLITO, Politecnico di Torino, *Corso Duca degli Abruzzi, 24, 10129 Torino - Italy, roberta.fusaro@polito.it*
[4] POLITO, Politecnico di Torino, *Corso Duca degli Abruzzi, 24, 10129 Torino - Italy, nicole.viola@polito.it*

Fig 1. STRATOFLY MR3 Vehicle.

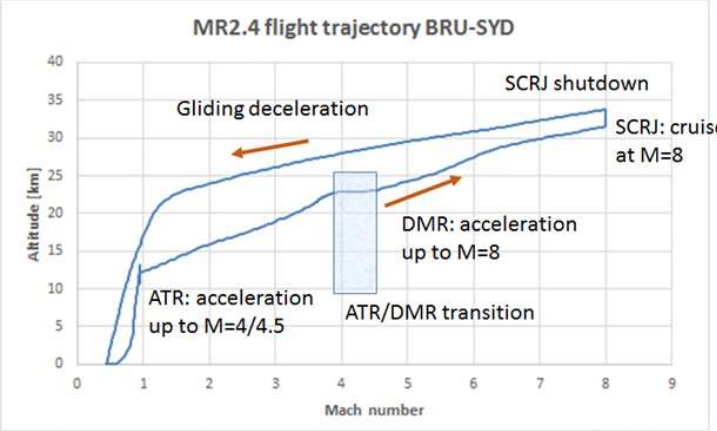

Fig 2. STRATOFLY mission profile.

2. Numerical Approach

The numerical tool used for the aerodynamic analysis of STRATOFLY vehicle is the VECC code (Viscous Effect on Complex Configurations) ([2]). It is essentially an extension of the S/HABP program (Supersonic/Hypersonic Arbitrary Body Program) with the adding of a GUI (Graphical User Interface) and adding/update of aerodynamic tool as stability derivatives, control surface deflection, boundary layer calculations (aero-heating). In this work, the aerodynamic coefficients have been obtained and used for the stability and trimmability analysis mainly with the hypothesis of inviscid fluid flow.

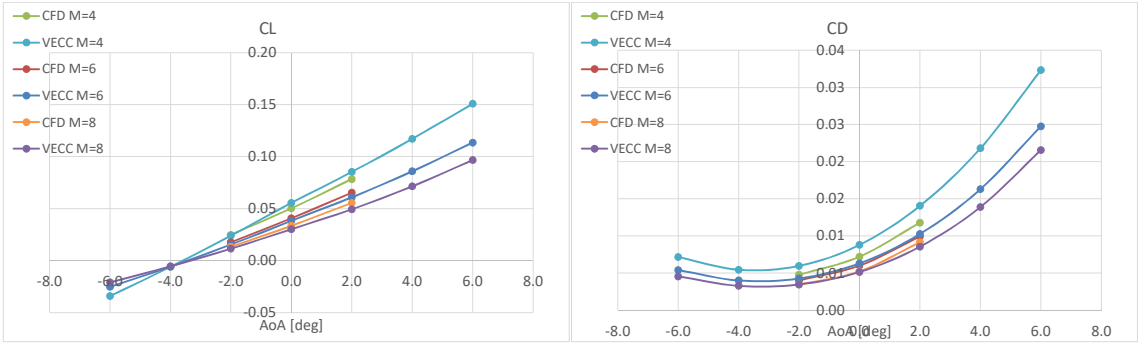

Fig 3. Comparison VECC vs CFD: CL (left) and CD (right) at Mach=4, 6, 8.

After having tuned the surface impact method with available CFD results by ESA and CIRA on the previous and very similar LAPCAT-II vehicle (Fig 3), and fixed the calculation strategy (tangent-wedge method for windside, Newtonian/Prandt-Meyer expansion for leeside and fuselage), the results have

been analysed in terms of aerodynamic performance, static stability (both longitudinal and lateral-directional), sensitivity to centre of gravity (CoG) movement, analysis of trimmability.

3. Numerical Results

In this section the aerodynamic analysis of STRATOFLY MR3 vehicle in supersonic and hypersonic range is reported, carried out by means of the engineering method described in previous section. Several configurations have been analyzed in order to find the stable and trimmable one.

3.1. Basic Configuration. Stability Analysis.

CIRA recalculated the AEDB for the MR3 vehicle in supersonic-hypersonic regime by using the surface impact method (SIM, i.e. the VECC code) and including the effect of control surfaces. In the following figures, some results are reported: the lift, drag and pitching moment coefficients (CL, CD, CM_y) in function of angle-of-attack in the supersonic-hypersonic range and the effect of elevons deflection on CM_y at M=8.

Table 1. Test Matrix for Basic Configuration.

Mach	AoA	AoS	Delta_Flap
1.5, 1.7, 2.0, 3.0, 4.0 5.0, 6.0, 7.0, 8.0	-6° -> 6° step 1°	-2°, 0°, 2°	-20° -> 20° Step 5°

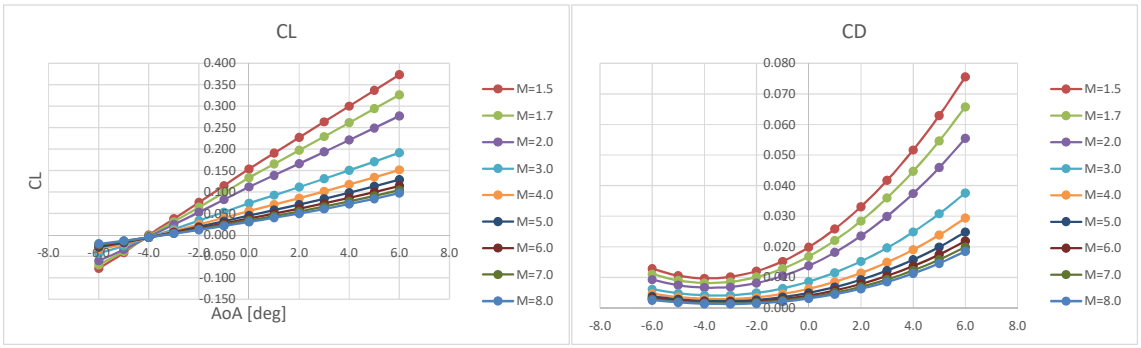

Fig 4: Lift and Drag coefficients.

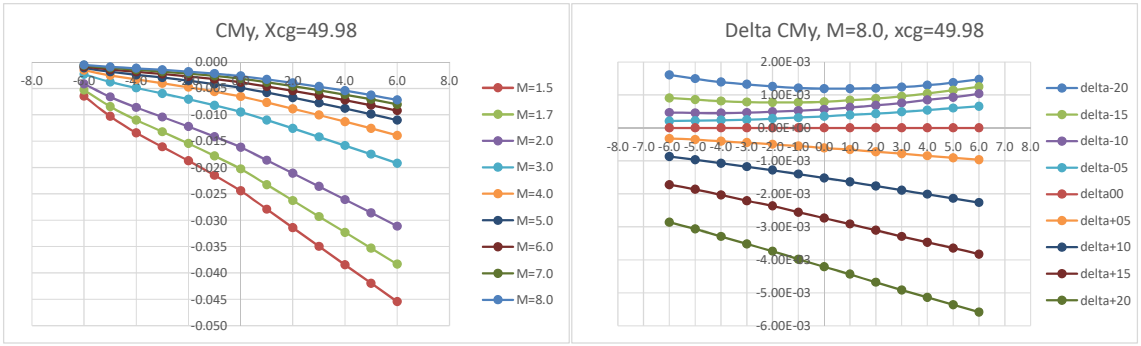

Fig 5: Pitching Moment coefficient and effect of elevon control surfaces at M=8.

A linear behaviour of CL in the AoA range is predicted (see Fig 4, left) while a classical quadratic one for the CD coefficient (see Fig 4, right), as well as a high lift-to-drag ratio of about 10 at AoA=0°, as expected by a waverider configuration. Moreover, Mach number independence of aerodynamic coefficients is still not fully reached at Mach=8. A clear longitudinal static stability ($Cm_\alpha<0$) at all Mach numbers for CoG values of Xcog=49.98m (with 20% fuel) is predicted (see Fig 5, left), with a decrease of stability with Mach number and with more backward CoG. It is clear the need for trimmability with negative elevon deflection for all flight conditions (large ΔCm to null, greater for lower Mach, see Fig 5, right), thus confirming the conflicting requirements: stability vs. trimmability. Of course, in present working hypotheses the beneficial engine-on effect on Cm (shift up of curve) is totally missing.

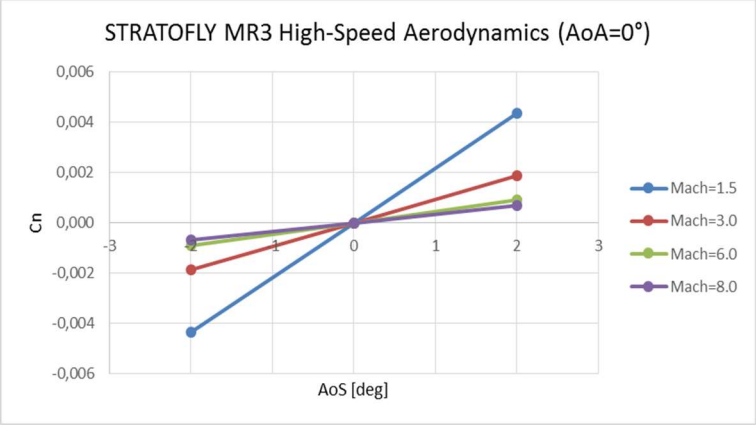

Fig 6. Yawing moment coefficient vs. AoS.

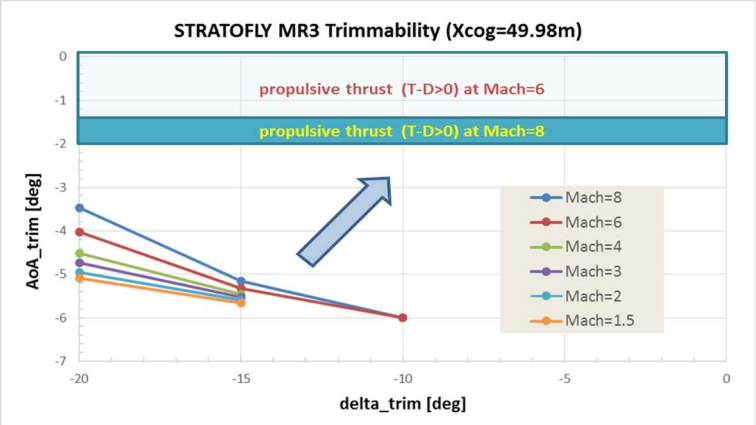

Fig 7. Trimmability map.

The MR3 vehicle clearly features a lateral-directional static stability (see Fig 6) which however decreases with Mach number and is not affected by the full AoA range [-6°÷6°], and with a very small effect of CoG movement on lateral stability (Cnβ>0). The predicted trimmability map of the MR3 vehicle (for the more forward CoG position), always reminding that we are dealing only with external surfaces (no propulsive flowpath accounted for, nor viscous effects), is shown in Fig 7. The trim AoA values are far from the optimum values emerged from the aero-propulsive analysis, i.e. maximum propulsive thrust for AoA=-2°÷0° at Mach=6 and AoA=-2° at Mach=8.

By the way, these are the results of the first design loop of the Flight Control System, and possible viable solutions to be investigated to get trim conditions for optimum propulsive thrust are: i) evaluate the effect of propulsive flowpath and motor-on on trimmability, ii) enlarge the horizontal control surfaces, iii) reconsider the canard wings, iv) change the elevon airfoil shape, and v) change the wing-body angle.

3.2. SIM AEDB. Trimmability Analysis

Three configurations have been analysed and compared in order to find the more appropriate in terms of trimmability and manoeuvrability. The analysis is conducted with reference to the centre of gravity.

The basic configuration

As we have seen in the previous section, the basic configuration is not trimmable in the range of angle of attack of interest (AoA> -2°), also at the maximum deflection of flap surfaces (see Fig 8). For example, the angle of trim is reported in the next Table 2 and Fig 9 for two flap deflection angles and several Mach numbers. As we can see, the trim angle of attack is always lower than -2°, so the vehicle is stable but not flyable at the desired angle of attack.

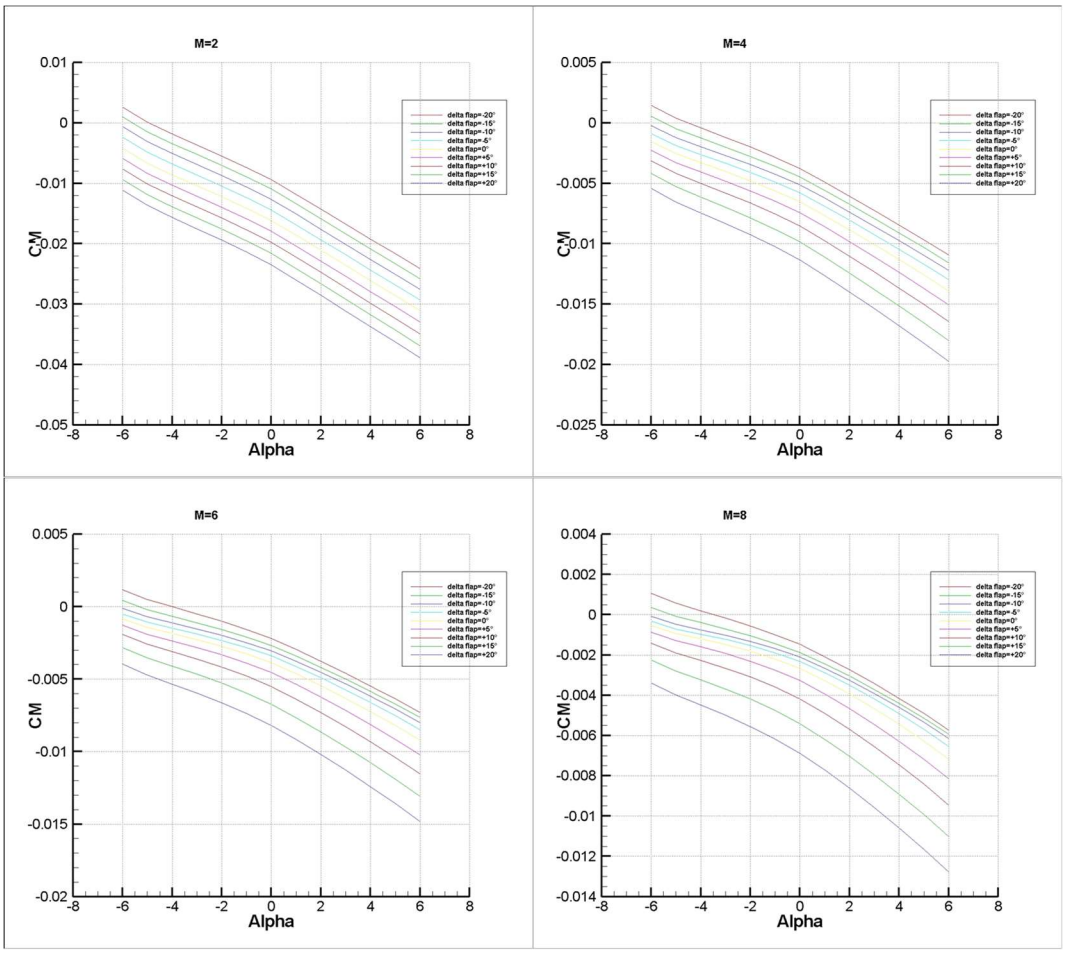

Fig 8. Pitching Moment for Basic Configuration at various Mach number and flap deflections.

Table 2. Angle of trim. Basic configuration with flaps activation.

	AoA trim		with flaps		
delta flap	M=1.5	M=2	M=4	M=6	M=8
-20	-5.091	-4.945	-4.512	-4.020	-3.472
-15	-5.660	-5.595	-5.461	-5.323	-5.159

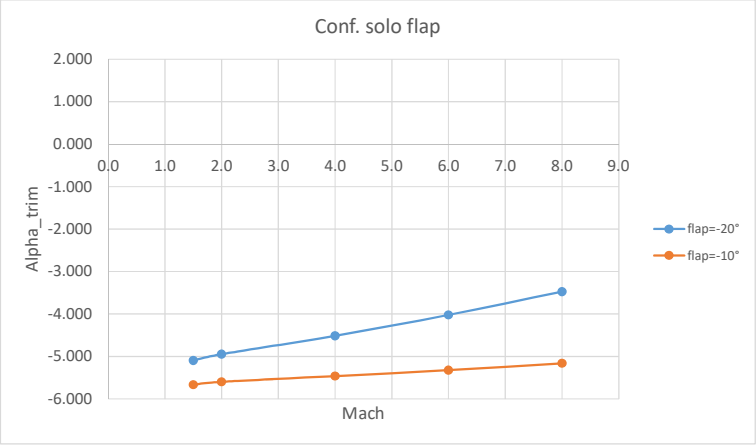

Fig 9. Trend of angle of trim. Basic configuration.

The canards configuration

In this section, we report the analysis of a configuration with the adding of canards control surfaces (see Table 3) located in front part of the fuselage (Fig 10). The surface area of each canard is 60 m^2.

As we can see from the next table and figure (Table 4, Fig 11), with the presence of canards the vehicle is trimmable at angle of attack greater than -2° with a large range of possible values. For example, for a given flap deflection of -20°, we can reach an angle of attack of 1.178 degrees at Mach= 1.5 and higher values at higher Mach number. With a flap deflection of -15° we are still able to trim the vehicle at the prescribed angle-of-attack AoA=-2°, but in general with a lower range of angle of trim.

Table 3. Test Matrix for Canards Configuration.

Mach	AoA	AoS	Delta_canards
1.5, 1.7, 2.0, 3.0, 4.0 5.0, 6.0, 7.0, 8.0	-6° -> 6° step 1°	0°	-20° -> 20° Step 5°

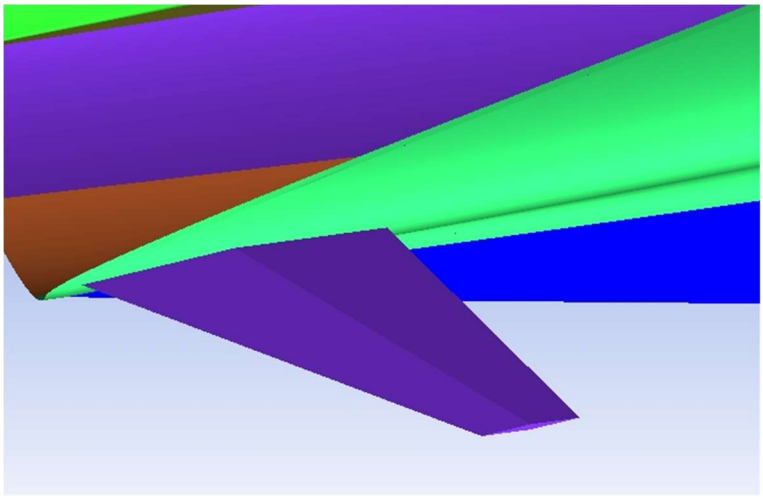

Fig 10. Canards Configuration.

Table 4. Angle of trim. Canards configuration. Flap=-20°, -15°

	AoA_trim		flap=-20°				AoA_trim		flap=-15°		
δ_c	1.5	2.0	4.0	6.0	8.0	δ_c	1.5	2.0	4.0	6.0	8.0
20	1.178	1.955	5.222			20	0.347	1.083	4.329		
15	-0.390	0.246	2.164	4.478		15	-1.503	-0.835	1.211	3.643	
10	-2.726	-2.159	-0.630	0.681	1.806	10	-3.988	-3.541	-2.195	-0.607	0.767
5	-5.133	-4.932	-4.204	-3.192	-2.050	5	-5.892	-5.827	-5.696	-5.525	-5.308
0						0					

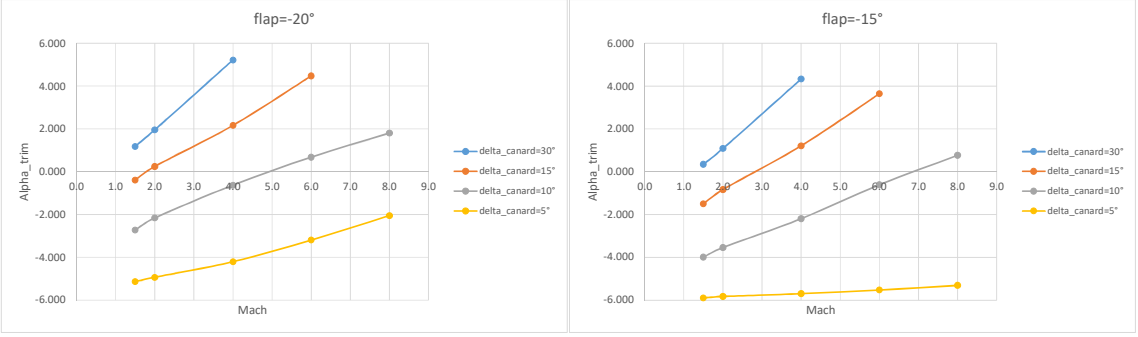

Fig 11. Trend of angle of trim. Canards configuration. Flap=-20°, -15°

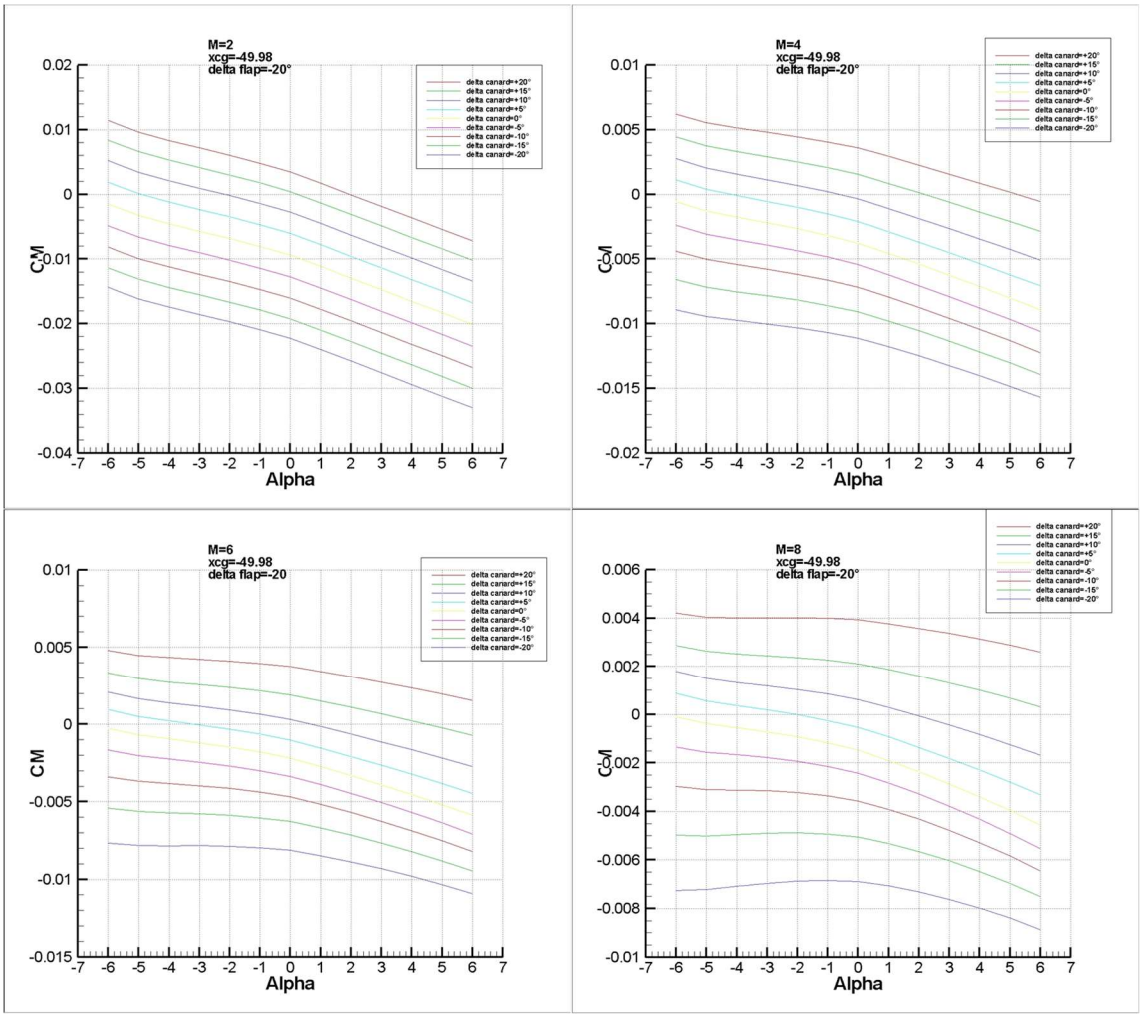

Fig 12. Pitching Moment coefficient for Canards at various Mach number and flap deflections.

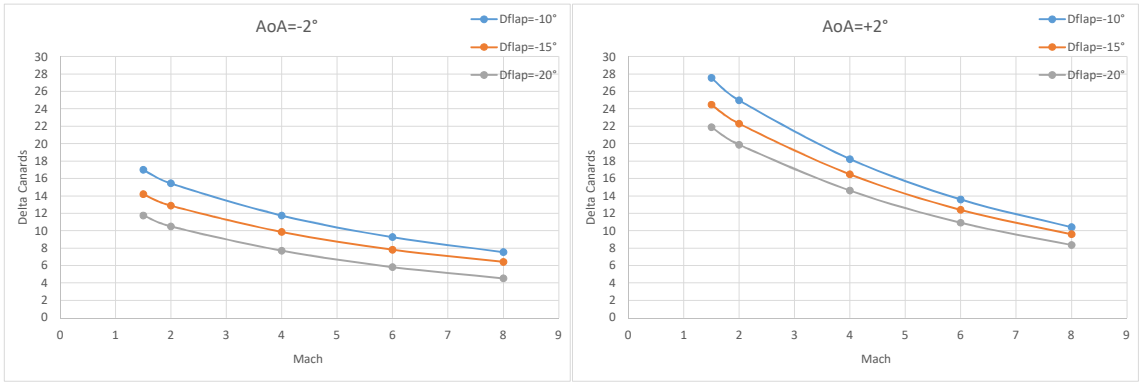

Fig 13. Delta canard vs Mach number for fixed angle of attack. AoA=-2°, 2°.

In Fig 12 we can see the effect of canards at several Mach numbers and for a flap deflection of -20° that is the maximum allowable. The effet of canards is to give a positive increment of pitching moment allowing the trim of the vehicle for this flap deflection and even for lower deflection if it. It is important to remark as the vehicle remains stable in the range of interest of angle of attack.

At the and of this section we report the delta canard necessary to trim the vehicle versus Mach number for several flap deflections, thus confirming the feasibility of this design (Fig 13).

The body-flap configuration

As an alternative to the Canards, a Body-Flap configuration has been taken into account in this section. In this configuration, an enlargement of the flaps was also applied (increasing of 50% of the chord, from 60 to 90 m^2 of total surface).

In Fig 14 the rear part of the vehicle is shown, where the body flap location and the new enlarged flaps can be observed. The two body-flaps are located on the rear upper part of the fuselage in-between the two vertical tails. The total surface area of the two body-flaps is of about 50 m^2.

Table 5. Test Matrix for Body-Flap Configuration.

Mach	AoA	AoS	Delta_Body_Flap
1.5, 1.7, 2.0, 3.0, 4.0 5.0, 6.0, 7.0, 8.0	-6° -> 6° step 1°	-2°, 0°, 2°	0° -> -30° Step 5°

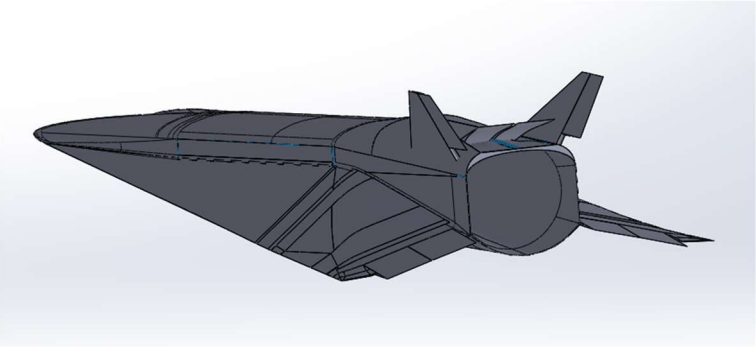

Fig 14. Body-Flap Configuration.

As we can see from next Table 6 and Fig 15, the Body-Flap configuration is able to trim the vehicle for the angle of attack of -2°, but provides a lower range of angle of attack for each Mach number with respect to the Canards configuration.

Comparing Table 4 with Table 6 (i.e. at the same flap angle of deflection, -20°) we can see that with Canards we have higher values of angle of trim, and also a larger range, and so a higher flexibility in manoeuvring.

In Fig 16 we can see the effect of body-flap at several Mach numbers and for a flap deflection of -20°. The effet is similar to that of canards (Fig 12) that is to give a positive increment of pitching moment but with a lower strength, allowing anyway the trim of the vehicle for this flap deflection.

Fig 17 shows the deflection of body flaps vs Mach number in the hypothesis of flying at an angle of attack of -2°. It has to be remarked that the flying is possible only if we operate with a flap deflection of -20°, that is the maximum one.

Table 6. Angle of trim. Body-Flap configuration. Flap=-20°, -10°

	AoA_trim		flap=-20°				AoA_trim		flap=-10°		
δ_b_f	M=1.5	M=2	M=4	M=6	M=8	δ_b_f	M=1.5	M=2	M=4	M=6	M=8
-30	-1.622	-1.069	0.300	1.225	1.904	-30	-4.141	-3.608	-1.898	-0.483	0.554
-25	-2.021	-1.557	-0.408	0.381	0.943	-25	-4.508	-4.118	-2.826	-1.675	-0.712
-20	-2.434	-2.030	-1.103	-0.425	0.073	-20	-4.876	-4.595	-3.721	-2.882	-2.098
-15	-2.830	-2.491	-1.737	-1.167	-0.716	-15	-5.196	-5.040	-4.505	-4.000	-3.489
-10	-3.196	-2.907	-2.267	-1.757	-1.339	-10	-5.480	-5.388	-5.136	-4.902	-4.667
-5	-3.525	-3.265	-2.683	-2.164	-1.714	-5	-5.737	-5.687	-5.557	-5.466	-5.392
0	-3.882	-3.602	-2.980	-2.415	-1.889	0	-5.989	-5.955	-5.867	-5.814	-5.771

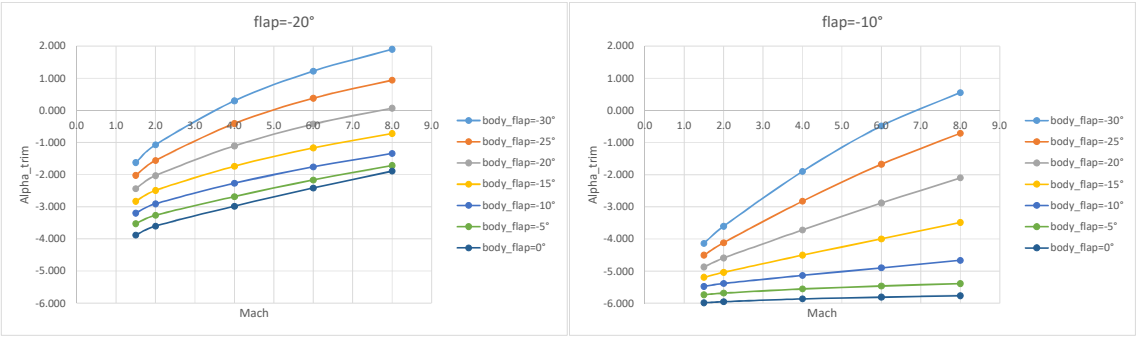

Fig 15. Trend of angle of trim. Body-Flap configuration. Flap=-20°, -10°

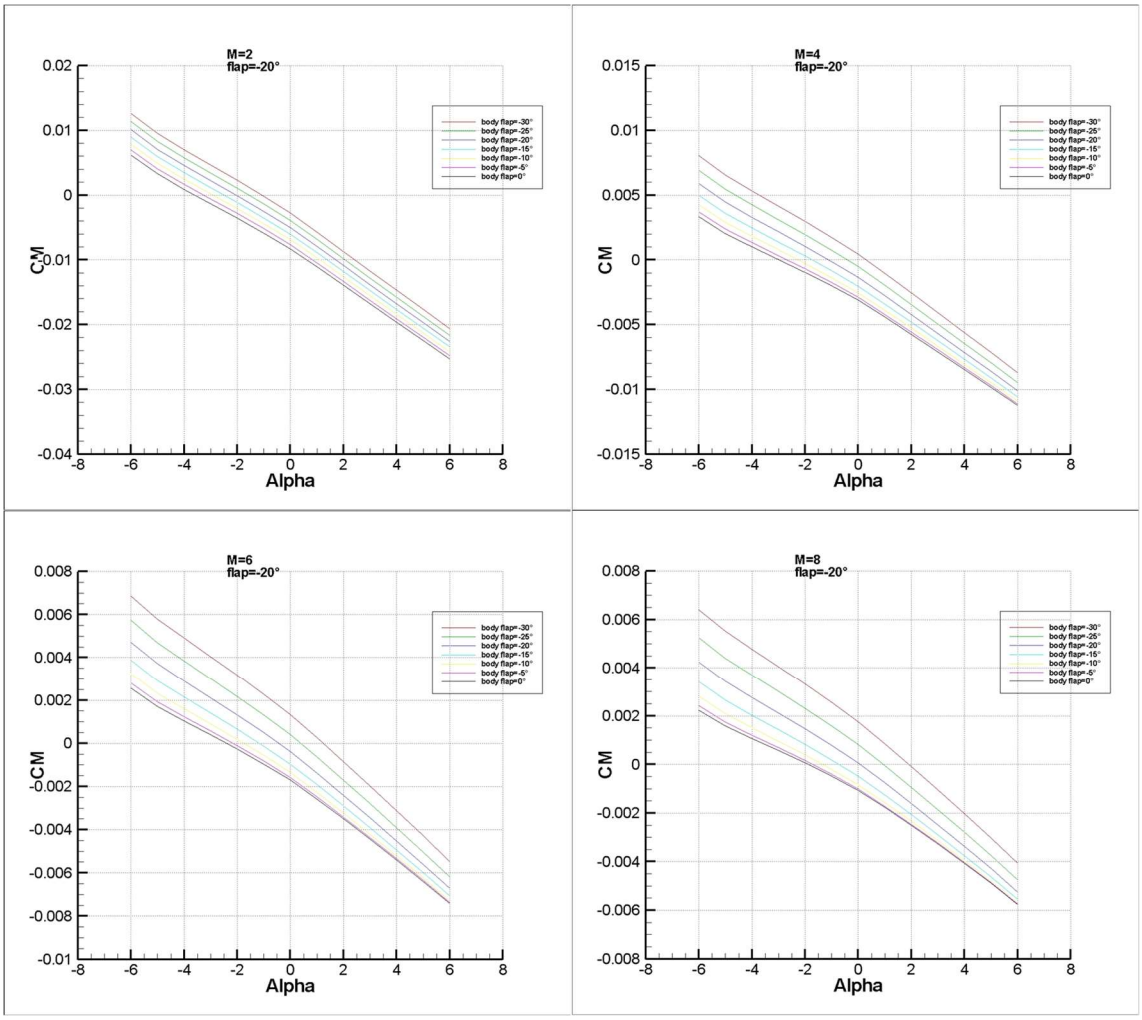

Fig 16. Pitching Moment coefficient for Body-Flap at various Mach number and flap deflections.

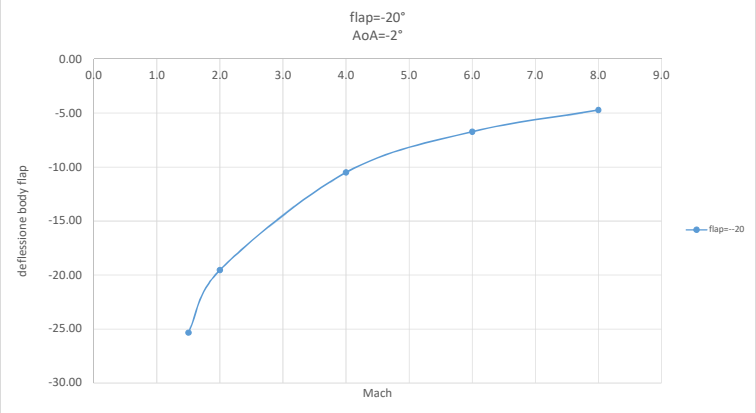

Fig 17. Body flap deflection vs Mach number at AoA=-2° and Flap=-20°.

4. CFD simulations

In this section an inviscid CFD analysis covering all the range of Mach number is reported. It was decided to use a low-fidelity CFD approach (inviscid simulations) instead of subsonic (incompressible) panel methods (PM) for two main reasons: unavailability of expertise and experience on using panel methods and the possibility to simulate flight conditions not covered by PM, and also for cross checking purposes.

An Eulerian unstructured grid of about one million of cells (half configuration) has been generated by means of ICEMCFD-TETRA grid generator (Fig 18) and the commercial code ANSYS-Fluent has been adopted for the numerical calculations. Based on past experiences with very similar problems ([13],[14]), the number of cells has been selected to guarantee a good compromise between CPU time and accuracy, and then a grid error lower than 10% is expected [13].

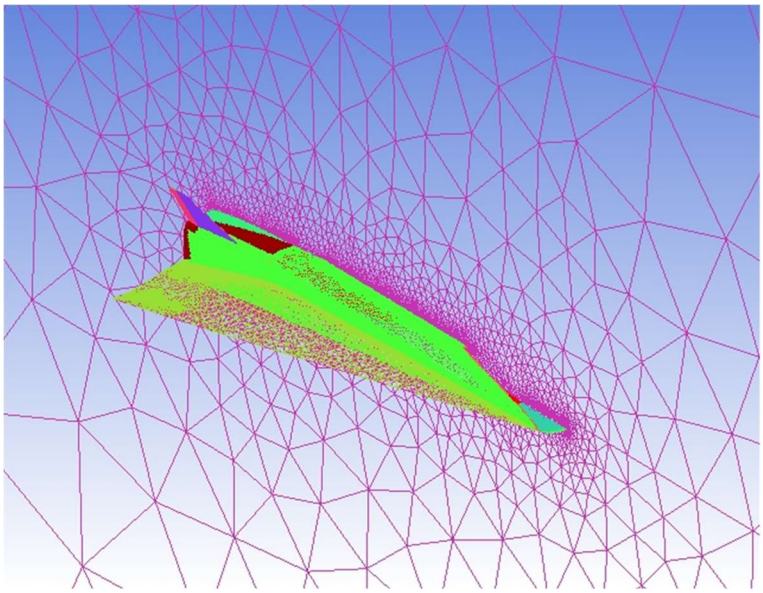

Fig 18. Inviscid Grid. Half body and symmetry plane. Cells = 1 M

Some outputs are reported in the Fig 19 and Fig 20, where the results of the inviscid external CFD simulations are compared with already available results previously obtained by means of Supersonic/Hypersonic Panels Method (Surface Impact Method tool), based on classical Modified-Newtonian, Tangent-Wedge, and Shock-Expansion Theories. In the supersonic-hypersonic range down to Mach = 3 the comparisons are good, at least for small angles of attack (i.e., the case reported in Figures 4 and 5). The discrepancy between the two methods is expected to increase for higher angles of attack. However, this is not the case for the STRATOFLY MR3 vehicle whose angle of attack throughout the mission is between −2° and +2°.

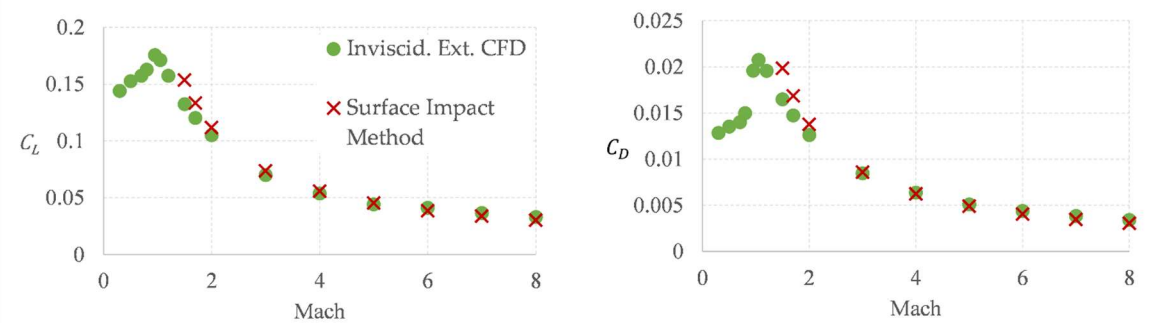

(a) (**b**)

Fig 19. Lift (a) and Drag (b) coefficients versus Mach at α = 0°.

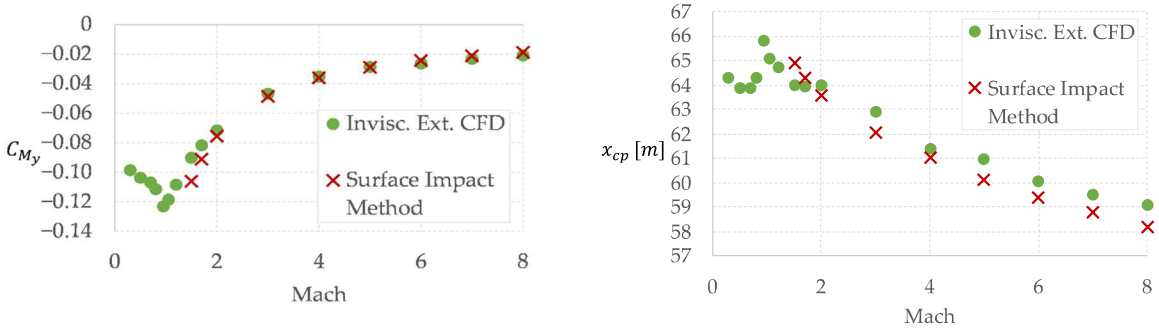

(a) (b)

Fig 20. Pitching Moment (a) and Centre of Pressure (b) versus Mach at α = 0°.

This section further exploits the CFD simulations already presented in the previous sections (that includes both the external and the internal domain of the vehicle) and provides suggestions on how to evaluate the contribution of the integrated propulsive flow path which consists of an intake, a combustor, and a nozzle, all embedded inside the wave-rider vehicle layout. As is reported in Fig 21, the flow-path substantially contributes to the overall aerodynamic forces, especially in subsonic, transonic, and low supersonic speed regimes. The main effects are the additional drag and a down-lift, both mainly due to the presence of the intake.

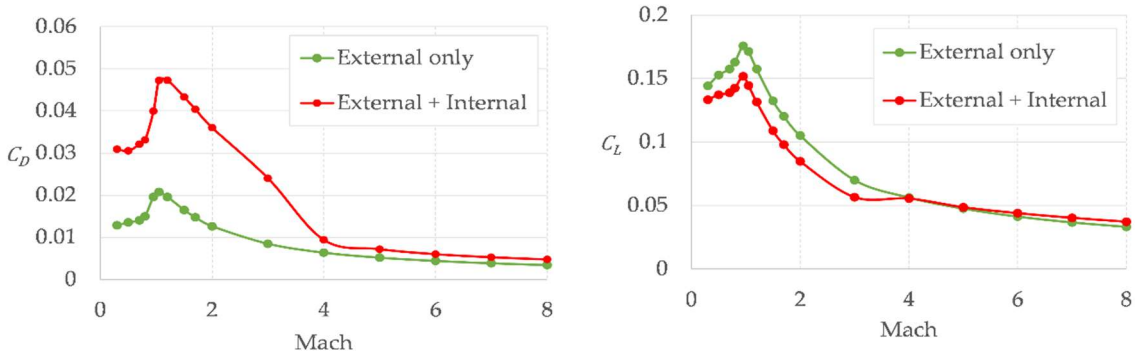

(**a**) (**b**)

Fig 21. Drag (a) and Lift (b) coefficients versus Mach at α = 0°. Comparison between full part and external part.

The sudden reduction of drag at M = 4 (Fig 22a) can be explained because the combustor swallows the shock wave, and in addition, the intake down-lift disappears (Fig 22b). The swallowing of the shock wave provides the aerodynamic characteristics with a hysteresis phenomenon, as can be seen in Fig 22. The investigated configuration shows that the shock wave is captured by the combustor between Mach 5 and Mach 6 during the ascent trajectory, while it is expelled between Mach 4 and Mach 3 during the descent trajectory. This different behavior of the air-intake can be noted in Fig 23 where we can see the Mach number contours at M = 4 and AoA = 0° far field conditions during ascent and descent

phases. However, looking at the envisaged in-flight operations of the MR3 propulsion subsystem, only the descending branch of the hysteresis graph has been considered. Indeed, the ATR ducts are expected to be open, thus facilitating the entrance of the shock wave into the combustor between Mach 3 and Mach 4.

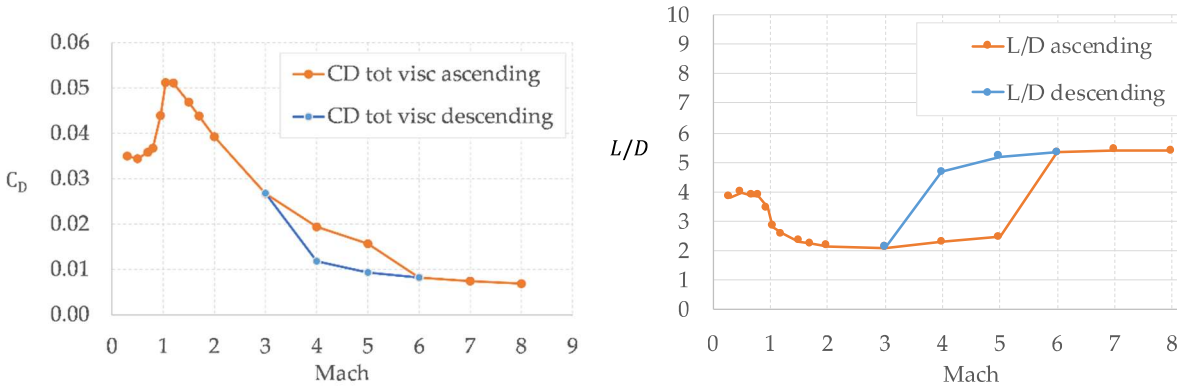

(a) (b)

Fig 22. Drag coefficient (a) and Lift-to-Drag ratio (b) versus Mach at α = 0°. Comparison between full part and external part.

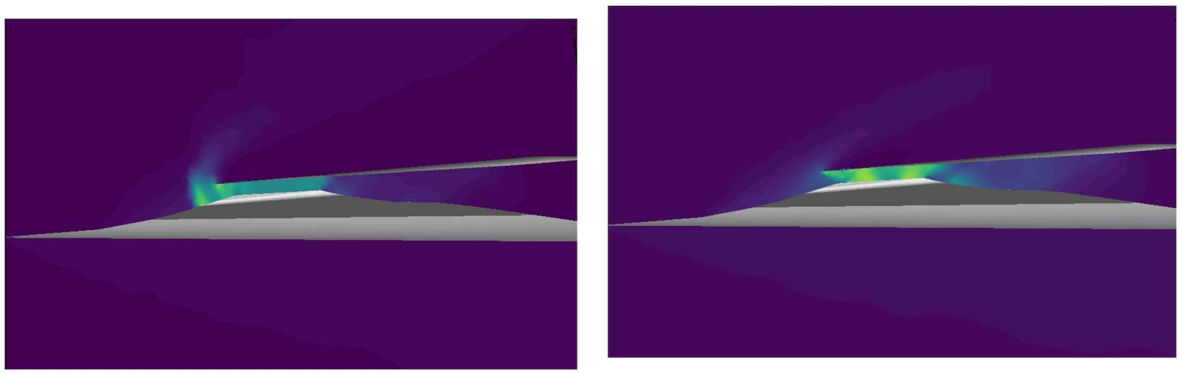

(a) (b)

Fig 23. Ascent (a) and Descent (b) Mach number contour on symmetry plane at M = 4 and α = 0° far field conditions.

It is important to note that all the internal flow path and the subsequent hysteresis phenomenon cannot be simulated by means of panels methods. Moreover, with CFD simulations it is also possible to conduct a full simulation of external and internal flow that is very important for a scramjet-propelled vehicle where aerodynamic and propulsion are strictly integrated. Additional activities, not reported here, have included also the combustion analysis and the nozzle thrust generation allowing the evaluation, in very efficient way, of the aeropropulsive balance (comparison between thrust and total drag) and the trajectory calculations ([15][16]).

5. Conclusions

An aerodynamic analysis of the STRATOFLY vehicle was conducted by means of engineering methods in the supersonic/hypersonic range and with CFD simulations in all the Mach number range in order to evaluate the stability and trimmability characteristics.

Several configurations were considered: one basic and two additional ones with the adding of canards and body-flaps.

The main conclusion is that the basic configuration is stable both longitudinally and laterally, but is not trimmable in the range of angle of attack of interest. Both alternative configurations, equipped with canards and body-flap, are able to obtain the desired angles of trim (i.e. $\alpha_{trim} > -2°$), giving the canards' one a wider range of fly-ability. It has to be said that in this work the effect of propulsion has not been

taken into account; being the line of thrust below the centre of mass, this effect is beneficial for what concerns the trimmability effect.

Inviscid CFD simulations have been also performed all over the range of Mach number showing a good cross check with the results of engineering methods for what concerns the external aerodynamic. These CFD analyses were large CPU time-consuming to converge and are in general more time-demanding for pre- and post-processing of data, but they are more reliable and can face up to more complex phenomena as the transonic regime, the internal flow path and the intake hysteresis behavior.

Acknowledgments

The H2020 STRATOFLY project has received funding from the European Union's Horizon 2020 research and innovation program under grant agreement No. 769246.

References

[1] Langener T., Erb S., Steelant J., "Trajectory Simulation and Optimization of the LAPCAT-MR2 Hypersonic Cruiser Concept", 29th Congress of the International Council of the Aeronautical Sciences (ICAS), September 7-12, 2014.

[2] Burns Keith A., Deters Kenneth J., Haley C.P., Kihlken Thomas A., "VECC, Software User's Manual", McDonnell Douglas Aerospace, WL-TR-95-3060, 1995.

[3] Murray, N., J. Steelant, and A. Mack. "Conceptual Design of a Mach 8 Hypersonic Cruiser with Dorsal Engine." Sixth European Symposium on Aerothermodynamics for Space Vehicles. Versailles, France, 2008.

[4] Murray N., Steelant J and Mack A. 2010. "Design Evolution for Highly Integrated Hypersonic Vehicles". Space Propulsion 2010, San Sebastian, Spain, 3-6 May 2010.

[5] Hannemann, K., S. Karl., J. Martinez Scharmm, and J. Steelant. "Methodology of a Combined Ground Based Testing and Numerical Modelling Analysis of Supersonic Combustion Flow Paths." Shock Waves, Vol. 20, No. 5 (Springer), 2010: 353-366.

[6] Karl, S. Numerical Investigation of a Generic Scramjet Configuration. Dissertation, TU Dresden, http://nbn-resolving.de/urn:nbn:de:bsz:14-qucosa-68695, 2011.

[7] Scheuermann, T., J. Chun, and J. von Wolfersdorf. "One-Dimensional Modelling of a Scramjet Combustor Reacting Flow." 15th AIAA International Space Planes and Hypersonic Systems and Technologies Conference. Dayton, OH: AIAA, 2008.

[8] Steelant, J. "Achievements obtained for sustained hypersonic flight within the LAPCAT project." 15th AIAA International Space Planes and Hypersonic Systems and Technologies Conference. Day-ton, OH: AIAA 2008-2578, 2008.

[9] Steelant, J. "Sustained Hypersonic Flight in Europe: Technology Drivers for LAPCATII." 16th AIAA/DLR/DGLR International Space Planes and Hypersonic System Technologies Conference. Bremen, Germany: AIAA 2009-7240, 2009.

[10] Vellaramkalayil, J., T. Langener, J. Steelant, and J. von Wolfersdorf. "Injector Layout Optimization for the LAPCAT MR2 Mach 8 Cruiser." AAAF-ESA-CNES Space Propulsion 2012. Bordeaux, France, 2012.

[11] Roncioni P., L. Cutrone, F. Battista, M. Marini, J. Steelant. "Preliminary Numerical Analysis of the LAPCAT MR2 Vehicle Configuration at Mach 8 Cruise Conditions". 4th European Conference For Aerospace Sciences (EU-CASS), Saint Petersburg, 4-8 July 2011.

[12] Langener T., J. Steelant, P. Roncioni, P. Natale, M. Marini. "Preliminary Performance Analysis of the LAPCAT-MR2 by means of Nose-to-Tail Computations". 18th AIAA International Space Planes and Hypersonic Systems and Technologies Conference. Tours, France, 2012.

[13] Roncioni, P.; Rufolo, G.C.; Votta, R.; Marini, M. An Extrapolation-To-Flight Methodology for Wind Tunnel Measurements Applied to the Prora-USV FTB1 Vehicle. In Proceedings of the 57th International Astronautical Congress, Valencia, Spain, 2–6 October 2006; doi:10.2514/6.IAC-06-D2.3.09.

[14] Rufolo, G.C.; Roncioni, P.; Marini, M.; Votta, R.; Palazzo, S. Experimental and Numerical Aerodynamic Data Integration and Aerodatabase Development for the PRORA-USV-FTB_1 Reusable Vehicle. In Proceedings of the 14th AIAA/AHI Space Planes and Hypersonic Systems and Technologies Conference, Canberra, Australia, 6–9 November 2006; doi:10.2514/6.2006-8031.

[15] Roncioni P., P. Natale, M. Marini, T. Langener, J. Steelant. "Numerical Simulations of the LAPCAT MR-2 Vehicle Scramjet Engine". 21st ISABE Conference, Busan, Korea, 9-13 September 2013.
[16] Roncioni P., P. Natale, M. Marini, T. Langener, J. Steelant. "Numerical Simulations and Performance Assessment of a Scramjet Powered Cruise Vehicle at Mach 8". Aerospace Science and Technology, vol. 42 (2015) pp. 218-228.
[17] Roncioni P., M. Marini, G. Saccone, R. Fusaro, N. Viola. "Preliminary Numerical Characterization of Stratofly Vehicle's Intake". FAR2019 Conference, Monopoli, Italy, 20 September - 3 October 2019.
[18] Viola N., Roncioni P., Gori O. and Fusaro R. "Aerodynamic Characterization of Hypersonic Transportation Systems and Its Impact on Mission Analysis", MDPI-energies https://doi.org/10.3390/en14123580, June 2021.